



An early fault detection method of series battery packs based on multi-feature clustering and unsupervised scoring



Wenhai Nie ^a, Zhongwei Deng ^{a,b,*} , Jinwen Li ^b , Kai Zhang ^b, Jingjing Zhou ^c, Fei Xiang ^c

^a School of Mechanical and Electrical Engineering, University of Electronic Science and Technology of China, Chengdu, 611731, China

^b College of Mechanical and Vehicle Engineering, Chongqing University, Chongqing, 400044, China

^c China Automotive Engineering Research Institute Co. Ltd., Chongqing, 401122, China

ARTICLE INFO

ABSTRACT

Keywords:

Lithium-ion battery
Unsupervised learning
Early fault warning
Fault detection
Hierarchical warning

With the rapid adoption of electric vehicles (EVs), ensuring the safety of power batteries is critical for reliable operation. Accurate assessment and early detection of lithium-ion battery faults are essential to prevent significant losses and safety incidents. However, accurately identifying and distinguishing potential faulty cells at an early stage remains challenging, as many existing methods fail to meet the requirements for real-time monitoring and reliability. To address these challenges, a novel early fault detection algorithm based on multi-feature clustering fusion for unsupervised scoring and hierarchical warning is proposed in this paper, aiming to detect, locate and tract battery fault cells in real-world scenarios. Initially, features characterizing early cell information from different perspectives are extracted. Then, unsupervised iterative scoring of battery cells is performed using clustering algorithms and a sliding window technique. Finally, a hierarchical warning mechanism for fault detection is implemented based on real-time scoring results and cumulative values to ensure high detection accuracy. The proposed algorithm is validated using three different datasets of early faults. It extends the warning time for abnormal cells by over ten days relative to battery management systems. This significantly enhances early fault detection capability, contributing to the safe and efficient operation of EVs.

1. Introduction

With the increasing consumption of fossil fuels and growing concerns about environmental protection, the electrification of transportation has emerged as a primary avenue for addressing these issues [1]. Electric vehicles (EVs), known for their clean energy and low pollution, have become a central focus of global energy reform. Nations around the world are implementing policies to secure a competitive edge, particularly in the power battery sector. For example, the United States and Europe are striving to localize lithium-ion battery supply chains [2], while China is investing in power battery supply chains in countries such as Mexico, Indonesia, and those in Africa to facilitate global green transformation and foster local economic development [3]. Moreover, Mexico is emerging as a regional hub for EV production, leveraging its policy advantages and manufacturing capabilities [4]. However, the rapid growth of the power battery industry has also heightened concerns about battery safety. As a vital component of EVs, lithium-ion batteries represent approximately 50% of the total vehicle cost, underscoring the critical importance of battery safety for safeguarding both lives and

property [5]. However, due to material defects, extreme operation, and improper use [6], batteries will inevitably experience failures such as capacity decay or internal short circuits (ISCs) during long-term operation [7]. For potential developing faults such as ISCs, accurate and timely fault detection in the early stages of battery malfunction allows for sufficient time to conduct prompt maintenance on the battery and prevent further deterioration. Hence, the early detection of battery faults holds significant importance for EVs [8]. However, in the early stage of faults, the electrical and thermal characteristics of faulty cells may not exhibit significant changes, making it difficult for the battery management system (BMS) to detect the occurrence of faults. Moreover, due to the relatively low sampling frequency of sensors in the battery system [9], relying on external characteristic data such as temperature and voltage for feature extraction and subsequent fault detection often leads to numerous misdiagnoses. Therefore, achieving early, accurate, and effective detection of battery faults remains a critical challenge to be addressed.

Battery faults can originate from a variety of causes, such as material defects arising during the manufacturing process, exposure to extreme

* Corresponding author. School of Mechanical and Electrical Engineering, University of Electronic Science and Technology of China, Chengdu, 611731, China.
E-mail address: dengzw1127@uestc.edu.cn (Z. Deng).

operating conditions, and improper usage [10]. From a control system perspective, battery system faults can be categorized into three main types: battery fault, sensor fault, and actuator fault. Among these, battery fault is the most critical and concerning fault. The process of battery fault detection involves utilizing collected sensor data to detect abnormalities within the system through diagnostic algorithms. This process also aims to identify the location of the abnormality and even the type of the fault [11]. Current methodologies for diagnosing faults in lithium-ion batteries can be classified into three categories: knowledge-based methods, model-based methods, and data-driven methods [12].

Knowledge-based methods for fault detection leverage existing knowledge and observed data of the battery system to diagnose faults. These approaches utilize methodologies such as fault trees, graph theory, fuzzy logic, and expert systems to achieve fault detection without the necessity of model establishment. Nevertheless, these methods heavily depend on understanding the mechanisms underlying battery faults and accumulating extensive knowledge and experience over time. Acquiring such knowledge and formulating rules for these methods can pose significant challenges [13]. Zhu et al. [14] conducted an analysis of the variation of voltage and temperature to achieve severity grading of battery overcharge faults.

Model-based fault detection methods, based on the physical or mechanistic models of batteries, typically compute the discrepancies between model predictions and sensor observations. These discrepancies are then compared with predefined thresholds to determine the presence of faults [15]. In general, model-based fault detection methods typically involve two main steps: residual generation and residual evaluation. In the residual generation process, there are primarily three methods: state estimation method, parameter estimation method, and odd-even space method. The state estimation approach [16] involves estimating the system's state based on available measurement data and comparing it with the model-predicted state to generate residuals indicating potential faults. The parameter estimation method [17] focuses on estimating parameters of the system model and generating residuals by comparing estimated parameters with measured parameters for fault detection. The odd-even space method constructs relationships between system inputs and outputs based on the system model, generating residuals by comparing actual system behavior with expected behavior derived from these relationships. Zhang et al. [18] proposed a technique for detecting and localizing multiple faults by constructing an equivalent circuit model of the battery pack. These methods can accurately describe the evolution of battery states under fault conditions. However, the model faces the following challenges: high precision requirement for input data, typically applicable to specific faults only; parameters obtained may inconsistently evolve with battery aging, and preset thresholds may become inapplicable over time [19].

Data-driven fault detection methods detect faults by directly analyzing and processing operational data, without relying on precise analytical models and expert experience [20]. Data-driven detection of lithium-ion battery faults simplifies the fault detection process by eliminating the need to consider complex fault mechanisms and system structures [21]. For instance, Hong et al. [22] employed Shannon entropy to detect temperature anomalies in battery packs, effectively predicting the occurrence time and location of temperature faults. Wang et al. [23] utilized a modified Shannon entropy to depict voltage evolution in individual cells, accurately forecasting the time and location of voltage faults within the battery pack. This method enabled real-time warnings and surpassed the limitations of traditional threshold techniques in identifying voltage anomalies within acceptable ranges. Qiao et al. [24] introduced a real-time online quantitative fault detection method for ISCs based on Incremental Capacity (IC) curves. Xia et al. [25] proposed a battery fault detection technique based on correlation coefficients to detect capacity inconsistencies among individual cells within a battery module. However, this method is limited in its ability to effectively diagnose other types of faults. Jiang et al. [26] suggested

employing the State Representation Methodology (SRM) to analyze voltage levels of all cells in actual vehicles, enabling the precise identification of voltage faults in individual cells.

Furthermore, with advancements in network communication and cloud storage technology, harnessing field data from EVs has become feasible. Qiao et al. [27] proposed a novel mean normalization technique to amplify the voltage characteristics of ISC cells within a battery pack. An adaptive Kalman filtering algorithm was utilized to filter the mean normalized values, thereby obtaining pronounced ISC features. This method can be applied to sparse data scenarios with 40-s intervals in cloud-based data environments. Li et al. [28] developed a hybrid neural network to estimate battery internal resistance and assess battery safety in real-world EVs by analyzing occurrences of abnormal internal resistance. Guo et al. [29] proposed an unsupervised health scoring (UHS) method for early detection of battery faults utilizing cloud-based data. Li et al. [30] proposed a comprehensive data-driven approach for battery capacity trajectory prediction based on degradation pattern recognition and health indicator inference, enabling proactive battery maintenance.

Despite these advancements, the randomness of vehicle operations and the lower sampling frequency due to cloud-based data transmission contribute to the complexity and sparsity of cloud-based battery data, which significantly differs from laboratory data. Additionally, cloud-based data such as battery voltage and temperature may not exhibit conspicuous variations in the early stages of the fault, posing an obstacle to fault detection. To address these issues, this study proposes a fault detection algorithm based on multi-dimensional feature clustering fusion for unsupervised scoring and hierarchical warning. By utilizing cell voltage data, fault related features are extracted from various perspectives and fused using clustering algorithms to comprehensively and accurately capture early fault characteristics. Additionally, an adaptive sliding window is employed to accumulate classification results over a period, converting discrete classification outcomes into continuous unsupervised scoring results, thereby mitigating the impact of random errors resulting from cloud-based data. Lastly, a two-level hierarchical warning strategy is employed to prevent misdetection from weak early fault signals. Comparing unsupervised scores with the first threshold identifies potentially faulty cells, while a cumulative sum strategy tracks fault progression, using the second threshold for final detection. The main contributions of this study include.

- (1) A fault detection framework is constructed, incorporating multi-feature clustering fusion, which enables early fault characteristics to be represented from multiple perspectives.
- (2) The clustering algorithm and adaptive sliding time window are utilized to transform the classification problem into a fault-free scoring problem.
- (3) A hierarchical warning strategy is proposed, wherein the accumulation of scoring results over a period of time is utilized to differentiate early faults from random errors, thereby preventing misdetection.
- (4) Validated using data from three faulty vehicles, with tens of days improvement compared to BMS fault detection time.

The remaining parts of this paper are arranged as follows: Section 2 describes the methodology of the proposed methods, including data preprocessing, feature extraction, unsupervised scoring, and hierarchical warning; the results and discussion of the fault detection are presented in Section 3; Section 4 concludes this paper.

2. Methodology

In order to facilitate the early detection of faulty cells, it is necessary to extract fault related potential features. Utilizing field data uploaded to the cloud, relevant features indicative of early faults are extracted from various perspectives, effectively characterizing the safety status of the

batteries. Following this, clustering algorithms are utilized to classify faulty cells. These results, combined with an adaptive sliding time window, yield comprehensive scores for each battery cell within the system. Based on these scores, a hierarchical warning strategy is implemented for the final fault detection.

2.1. Main framework

The main framework of the proposed lithium-ion battery early fault detection algorithm is illustrated in Fig. 1. During the operation of EVs, the battery system generates a large amount of data, which is promptly uploaded to the cloud platform. The proposed method for detecting abnormal battery cells is deployed on a cloud platform, including data collection, data cleaning, feature extraction, unsupervised scoring, and hierarchical warning. Prior to obtaining the feature set, preprocessing is applied to the cloud data collected during the data acquisition stage. Significant outliers are removed from the raw data and replaced with the average values of the same row data, then abnormal cells can be detected based on unsupervised scoring results, and corresponding warning signals can be sent to the vehicle. Additionally, maintenance information can be generated based on hierarchical warning results and transmitted to the manufacturer or control center to guide timely maintenance of the battery systems. The core components of the proposed method are feature extraction, unsupervised scoring and hierarchical warning, as described in the following sections.

2.2. Feature extraction and analysis

To achieve real-time and comprehensive fault detection of the battery system, and to identify faulty cells at an early stage, it is essential to select appropriate fault-related features. The feature extraction needs to

adapt to sparse data from the cloud, ensuring that features can be extracted at any stage of EVs, whether during charging or driving, to support real-time fault detection. The extracted features should comprehensively characterize the safety status of the battery from multiple perspectives. To achieve this goal, three types of features are selected to construct the feature set in this study: Shannon entropy feature, Cell state value feature, and Extended root mean square error (RMSE). A detailed explanation of the definition and rationale behind the selection of these features will be provided in the following section.

In this paper, feature extraction is performed based on the cell voltage data. The cell voltage is represented as an $n \times m$ matrix $U_{n \times m}$:

$$U_{n \times m} = \begin{bmatrix} v_{1,1} & \dots & v_{1,m} \\ \dots & \dots & \dots \\ v_{n,1} & \dots & v_{n,m} \end{bmatrix} \quad (1)$$

where m represents the number of cells and n represents the number of sampling points.

(1) Shannon entropy: Shannon entropy proposed by Laude Elwood Shannon in 1948 [31] has been widely applied in thermodynamics, information science and other fields, and mainly used to judge the degree of disorder system. In order to enable real-time fault detection using Shannon entropy, Wang et al. [23] made modifications to the entropy calculation. The specific calculation process is shown below:

Form matrix $A_{k \times m} \in U_{n \times m}$ of cell voltage and obtain two extrema of matrix A:

$$\begin{aligned} x_{\min} &= \min\{x(i,j) | j = 1, 2, 3, \dots, k; i = 1, 2, 3, \dots, m\} \\ x_{\max} &= \max\{x(i,j) | j = 1, 2, 3, \dots, k; i = 1, 2, 3, \dots, m\} \end{aligned} \quad (2)$$

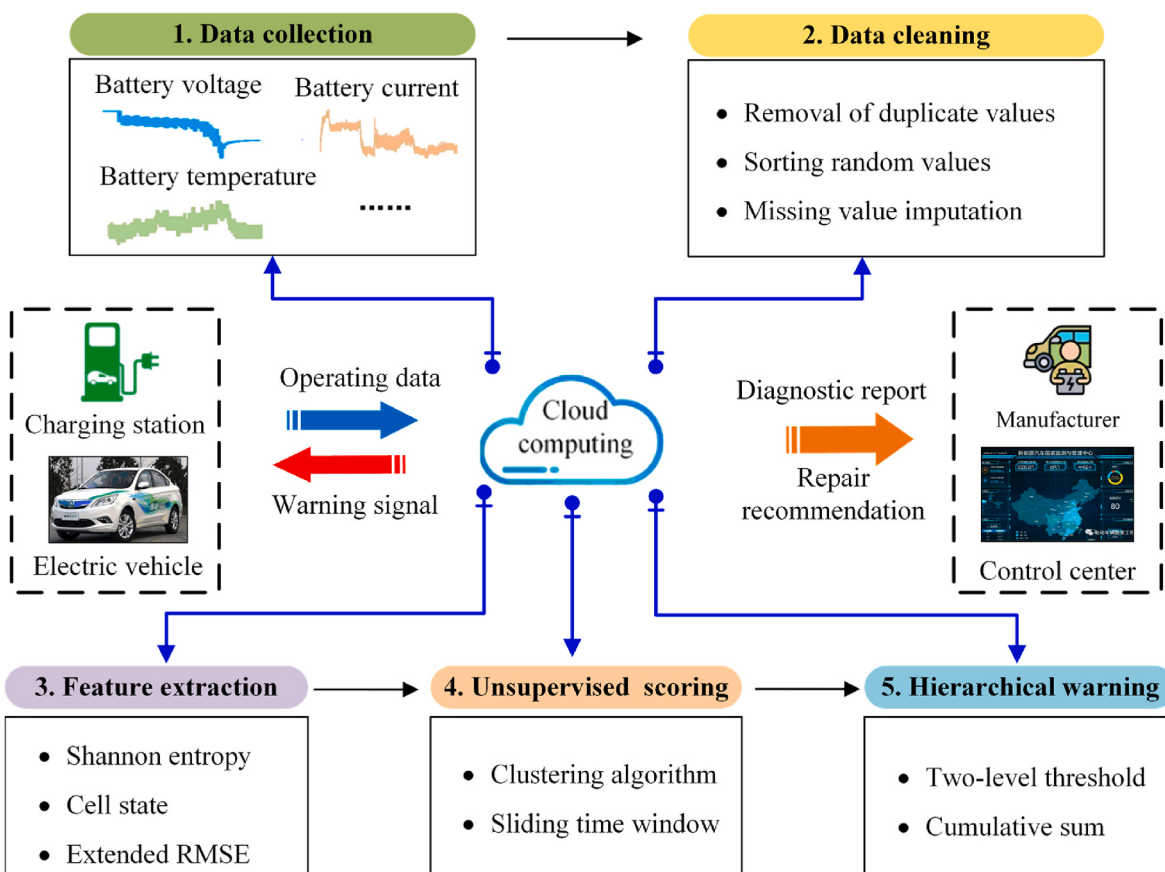


Fig. 1. Schematic representation of the proposed method.

where m is the number of battery cells in the battery pack; k is the sliding time window length.

Calculate the frequencies of each interval:

$$P = \begin{bmatrix} p_{1,1} & \dots & p_{1,m} \\ \dots & \dots & \dots \\ p_{l,1} & \dots & p_{l,m} \end{bmatrix} \quad (3)$$

where b_{ij} is the number of $x \in (x_{\min} + \lambda \frac{x_{\max} - x_{\min}}{l}, x_{\min} + (\lambda + 1) \frac{x_{\max} - x_{\min}}{l})$;

l is the number of the interval, $\lambda = 0, 1, 2, \dots, l$; $p_{ij} = \frac{b_{ij}}{\sum_{j=1}^l b_{ij}}$.

After performing the aforementioned calculations, the Shannon entropy value H_{ji} for the j -th sampling instant of the i -th cell can be obtained. By repeating this process, the Shannon entropy values for all battery cells can be obtained, as shown in the following equation:

$$H_j = [H_{j1} \dots H_{ji} \dots H_{jm}] \quad (4)$$

where $H_{ji} = -\sum_{j=1}^l p_{ij} \log p_{ij}$; H_j represents the Shannon entropy values for all individual battery cells at the j -th sampling instant.

(2) Cell state value: The SRM algorithm has been widely applied in various fields [26] such as bridges, road networks, and biomedical research, enabling the accurate determination of the health status of complex systems by revealing the relationship between monitoring data and system states. Therefore, the feature of cell state value can effectively reflect the overall changes in the battery system.

If the system's response x and the state function $f(\bullet)$ are known, the structural coefficient λ and the state variable ξ of the system can be derived. Furthermore, as time progresses, a new response x_{new} can be obtained. If the condition $f(\lambda, x_{new}) = \xi$ still holds, it indicates that the system remains unchanged. Otherwise, it suggests that the system has undergone changes.

$$\xi = f(\lambda, x) \quad (5)$$

As shown in Fig. 2, first, the length of the time window n is selected. Then, the feature matrix X_j is constructed for each time window, and the reference feature matrix G_j is determined. Using the SRM algorithm, the standard state ζ_1 of each battery cell and its corresponding λ are calculated using the initial data. Finally, the cell state value ζ_j for each time window is computed based on the λ .

(3) Extended RMSE: The Extended RMSE is distance-based fault characterization formulas, which can well identify the inconsistency evolution process in battery packs and recognize the voltage change after a certain delay when a micro-short circuit fault occurs in the battery. Due to the sensitivity of Extended RMSE to sampling errors from sensors, a method involving a sliding time window of length N has been employed to mitigate the impact of sampling errors. The Extended RMSE can be calculated by Eq. (6):

$$\begin{cases} U_t = (v_{t1}, v_{t2}, v_{t3}, \dots, v_{tm}) \\ G_{ji} = \frac{1}{N} \sum_{t=j-N}^j \left(v_{ti} - \frac{1}{m} \sum_{i=1}^m v_{ti} \right)^2 \\ G_j = [G_{j1} \dots G_{ji} \dots G_{jm}] \end{cases} \quad (6)$$

where m is the number of battery cells in the battery pack; U_t represents the original voltage of the battery cell at the t -th sampling time; v_{ti} represents the i -th cell voltage of at the t -th sampling time; G_{ji} represents the Extended RMSE of the i -th battery cell at the j -th sampling time and G_j represents the Extended RMSE of all battery cells at the j -th sampling time.

In summary, the aforementioned three types of features provide multiple perspectives on the safety status of battery cells, including fault information, discrepancies among faulty cells, and the degree of abnormalities in faulty cells. Therefore, the feature set can be obtained as shown in Eq. (7).

1. The length of the time window: n

$n = n$ sampling moments

2. Constructing the state matrix for each window

$$X_j = (x_1^j, \dots, x_i^j, \dots, x_n^j)^T = \begin{bmatrix} u_{11}^j, \dots, u_{1i}^j, \dots, u_{1m}^j \\ \vdots \\ u_{i1}^j, \dots, u_{ii}^j, \dots, u_{im}^j \\ \vdots \\ u_{n1}^j, \dots, u_{ni}^j, \dots, u_{nm}^j \end{bmatrix}$$

$$u_i^j = (u_{1i}^j, \dots, u_{ii}^j, \dots, u_{ni}^j)^T$$

$$G_j = X_j^T \times X_j = \begin{bmatrix} < u_1^j, u_1^j >, \dots, < u_1^j, u_i^j >, \dots, < u_1^j, u_m^j > \\ \vdots \\ < u_i^j, u_1^j >, \dots, < u_i^j, u_i^j >, \dots, < u_i^j, u_m^j > \\ \vdots \\ < u_m^j, u_1^j >, \dots, < u_m^j, u_i^j >, \dots, < u_m^j, u_m^j > \end{bmatrix}$$

3. Determining the reference parameter vector and reference state

$$\text{Objective function: } \min \left\| (I - \frac{1}{m} e^T e) G_1 \lambda \right\|^2$$

$$\text{Constraint conditions: } \sum_1^m \lambda_i = 1 \quad 0 \leq \lambda_i \leq 1$$

Reference parameter vector:

$$\zeta_1 = f(\lambda, x) = \sum_1^m \lambda_i < u_i^1, X_1 > = G_1 \times \lambda = (\zeta_{11} \dots \zeta_{1i} \dots \zeta_{1m})$$

4. Determination of states for each window

$$\zeta_j = f(\lambda, x) = \sum_1^m \lambda_i < u_i^j, X_j > = G_j \times \lambda = (\zeta_{j1} \dots \zeta_{ji} \dots \zeta_{jm})$$

Fig. 2. The calculation process of SRM.

$$\begin{cases} H_j = [H_{j1} \cdots H_{ji} \cdots H_{jm}] \\ \zeta_j = [\zeta_{j1} \cdots \zeta_{ji} \cdots \zeta_{jm}] \\ G_j = [G_{j1} \cdots G_{ji} \cdots G_{jm}] \end{cases} \quad (7)$$

2.3. Unsupervised health scoring method

The feature set proposed in section 2.2 can describe the fault state of each cell in the battery pack independently from multiple perspectives. Due to the polarization characteristics inherent in the battery and the stochastic nature of its operational conditions, these features exhibit varying responses across different time scales. Their combination can better describe the status of batteries.

Firstly, each feature within the feature set is normalization to mitigate the impact of magnitude discrepancies, thereby forming a normalized feature set. Next, the clustering algorithm is utilized with the normalization feature set to classify the battery cells. Then, a sliding time window is utilized for iterative scoring. Finally, the hierarchical warning strategy is employed, utilizing the results of unsupervised scoring compared with fixed thresholds to identify cells with a higher probability of fault occurrence. Subsequently, these cells are tracked using a cumulative sum strategy to assess whether faults continue to develop or worsen over time, leading to a final fault detection.

(1) Normalization: Owing to the diverse units of measurement for individual features, direct comparisons become challenging. Hence, it becomes imperative to standardize each feature, mitigating the impact of disparate features. Employing the Min-Max Scaling method, normalized scores for each feature are calculated, as depicted in Eq. (8):

$$\begin{cases} Z_{ji}^1 = \frac{H_{ji} - \min\{H_j\}}{\max\{H_j\} - \min\{H_j\}} \\ Z_{ji}^2 = \frac{\zeta_{ji} - \min\{\zeta_j\}}{\max\{\zeta_j\} - \min\{\zeta_j\}} \\ Z_{ji}^3 = \frac{G_{ji} - \min\{G_j\}}{\max\{G_j\} - \min\{G_j\}} \end{cases} \quad (8)$$

where Z_{ji}^1 represents the normalization score for the Shannon entropy of the i -th battery cell at the j -th sampling time; Z_{ji}^2 represents the normalization score for the Cell state value of the i -th battery cell at the j -th sampling time; Z_{ji}^3 represents the normalization score for the Extended RMSE of the i -th battery cell at the j -th sampling time.

Therefore, the normalization feature set can be obtained as shown in Eq. (9):

$$\begin{cases} Z_j^1 = [Z_{j1}^1 \cdots Z_{ji}^1 \cdots Z_{jm}^1] \\ Z_j^2 = [Z_{j1}^2 \cdots Z_{ji}^2 \cdots Z_{jm}^2] \\ Z_j^3 = [Z_{j1}^3 \cdots Z_{ji}^3 \cdots Z_{jm}^3] \end{cases} \quad (9)$$

(2) Cluster algorithm: The Density-Based Spatial Clustering of Applications with Noise (DBSCAN) algorithm is advantageous in that it does not require the user to input the number of clusters in advance, making it suitable for datasets with unknown or varying cluster numbers. Additionally, it is capable of capturing clusters with different densities and sizes, making it versatile for various types of data. Hence, the DBSCAN algorithm is highly suitable for the objectives of this research. The DBSCAN algorithm is characterized by two key parameters, the ϵ -neighborhood value (Eps) and the density threshold ($MinPts$). The computational process of DBSCAN is illustrated as follows. The clustering schematic is shown in Fig. 3.

- Step 1 Select an unexamined data point denoted as p from the dataset, ensuring that it has not been assigned to any cluster or labeled as noise.
- Step 2 Inspect the neighborhood: For the selected data point p , inspect its neighborhood (the region closes to p in terms of distance). If the number of points in the neighborhood is not less than the specified minimum points ($MinPts$), establish a new cluster C and add all points in the neighborhood to the candidate set G . If the number of points in the neighborhood is less than $minpts$, label point p as noise.
- Step 3 For unprocessed data points q in the candidate set G , inspect its neighborhood. If the number of points in the neighborhood is not less than $minpts$, add these points to G . If q has not been assigned to any cluster, include q in cluster C .
- Step 4 Repeat Step 3, continue to inspect unprocessed data points in the candidate set G and add qualifying points to cluster C .
- Step 5 Repeat Steps 1 to 4 until all data points are assigned to a cluster or labeled as noise.

After the above steps, one clustering result can be got for each clustering. When a cell is recognized as an outlier by the clustering algorithm, it is assigned a value of 1.

$$\begin{cases} Q_{ji} = \begin{cases} 0, p \text{ is a non-outlier} \\ 1, p \text{ is an outlier} \end{cases} \\ Q_j = [Q_{j1} \cdots Q_{ji} \cdots Q_{jm}] \end{cases} \quad (10)$$

where Q_{ji} represents the clustering result of the i -th battery cell at the j -th sampling time; Q_j represents the clustering result of all battery cells at the j -th sampling time.

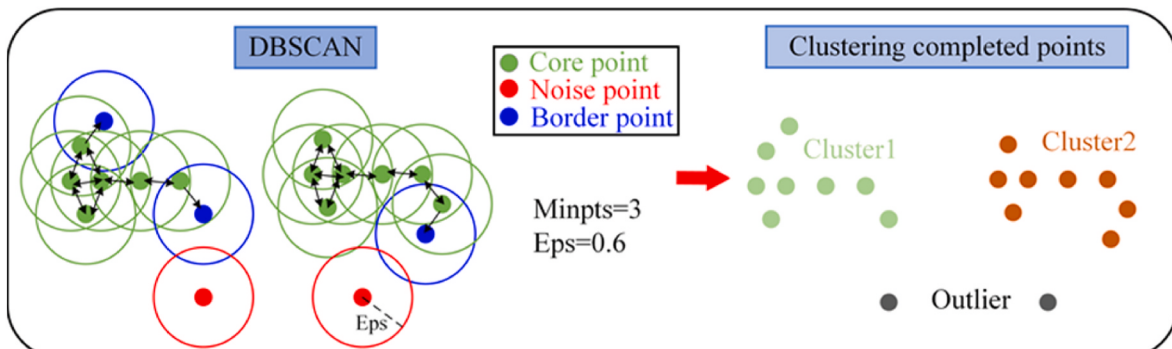


Fig. 3. DBSCAN algorithm schematic diagram.

(3) Unsupervised scoring: In this study, the iterative cumulative scoring method is employed to process the classification sequences generated by the clustering algorithm. A sliding window of length L is utilized, with each slide advancing by a step size of 1. This approach enables real-time processing of extensive data sequences and the generation of corresponding scoring results.

$$\begin{cases} F_{ji} = \frac{1}{L} \sum_{t=j-L}^j Q_{ti} \\ F_j = [F_{j1} \dots F_{ji} \dots F_{jm}] \end{cases} \quad (11)$$

where Q_{ti} represents the clustering result of the i -th battery cell at the t -th sampling time; F_{ji} represents the score of the i -th battery cell at the j -th sampling time; F_j represents the scores of all the battery cell at the j -th sampling time.

2.4. Hierarchical warning strategy

As depicted in Fig. 4, to enhance the credibility of diagnostic results and avoid misdetection in early fault detection, a hierarchical warning strategy is adopted, leveraging unsupervised scoring results F_{ji} compared against predetermined threshold_1 to pinpoint cells with a heightened likelihood of fault occurrence, thus initiating a Level I warning for timely intervention. Subsequently, these cells are monitored using the

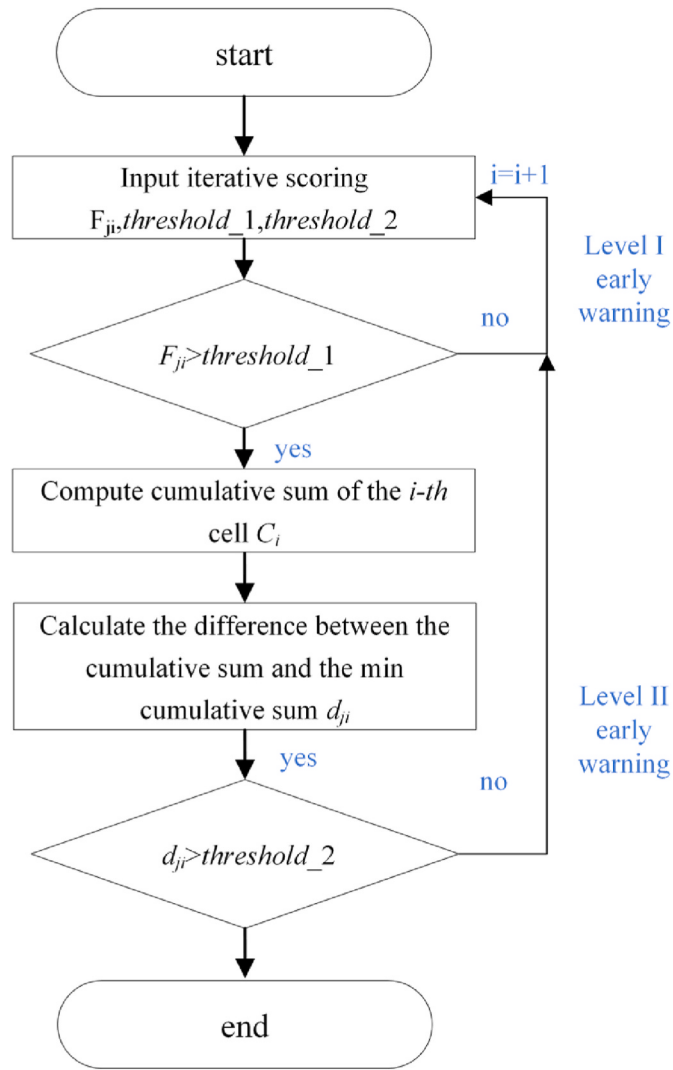


Fig. 4. Hierarchical warning strategy flowchart.

cumulative sum algorithm to ascertain if faults persist or deteriorate over time, culminating in a definitive fault detection. The calculation process is illustrated as shown in Eq. (12). Compare the difference results d_{ji} between the calculated cumulative sum and the minimum cumulative sum with the threshold_2 , thus initiating a Level II warning.

$$\begin{cases} C_{ji} = \sum_{t=1}^j F_{ti} - \text{threshold_1} \\ C_i = [C_{1i} \dots C_{2i} \dots C_{ji}] \\ d_{ji} = C_{ji} - \min\{C_i\} \\ \text{alarmII} = \begin{cases} 0, d_{ji} < \text{threshold_2} \\ 1, d_{ji} > \text{threshold_2} \end{cases} \end{cases} \quad (12)$$

where C_{ji} represents the cumulative sum of the i -th battery cell at the j -th sampling time; C_i represents the cumulative sum of the i -th battery cell; d_{ji} represents the difference between the cumulative sum and the minimum cumulative sum of the i -th battery cell at the j -th sampling time.

3. Results and discussion

To validate the effectiveness of the proposed method, this study selects a vehicle involved in no faults and three typical vehicles involved in faults. The information of these four vehicles is shown in Table 1, and the data is sourced from the National New Energy Vehicle Monitoring and Management Center (NMMC-NEV). Fault information was confirmed through expert analysis. Car1 has no faults, while Car2 experiences thermal runaway due to the worsening degree of ISC in cell #83, and Car3 undergoes thermal runaway due to the relatively high long-term self-discharge levels in cells #3 and #82. Car4 experiences an increase in internal resistance and an abnormal decrease in capacity in cell #64. All three accident vehicles eventually trigger thermal runaway, attributed to the delayed detection of minor voltage deviations in the early battery fault. Additionally, we have chosen multiple sample periods to verify the adaptability of the algorithm.

3.1. Fault detection based on different features

To assess the effectiveness of the proposed method, historical data from four operational EVs are used for testing. The voltage resolution of the on-board power batteries is set to 1 mV. Fig. 5 illustrates the voltage variation curves of each cell within the battery pack during the EV's operation. The gray curve represents the fault-free cells, while the red and blue curves represent the faulty cells.

Fig. 5(a) displays the voltage curves of Car1. It can be observed that the voltage variation curve under the actual working condition exhibits random perturbations, which may impact the fault detection accuracy. Fig. 5(b) presents the voltage curves of Car2. It is evident that the voltage of cell #83 is gradually deviating from the normal voltage. This indicates an increasing severity of the fault. At the 4000th sampling point, there is a sharp drop in the voltage of the battery cell #83. However, expert analysis confirms that this voltage drop is caused by deep discharge rather than a fault.

Fig. 5(c) illustrates the voltage curves of Car3. The red curve represents the voltage curve of battery cell #3, while the blue curve represents the voltage curve of battery cell #82. The voltages of these two

Table 1
Parameters of studied cars.

Vehicle number	Sample size	Sample period	Cell number	Faulty cell
Car1	65667	1s	96	no
Car2	14286	30s	89	#83
Car3	46868	10s	88	#3, #82
Car4	14973	30s	88	#64

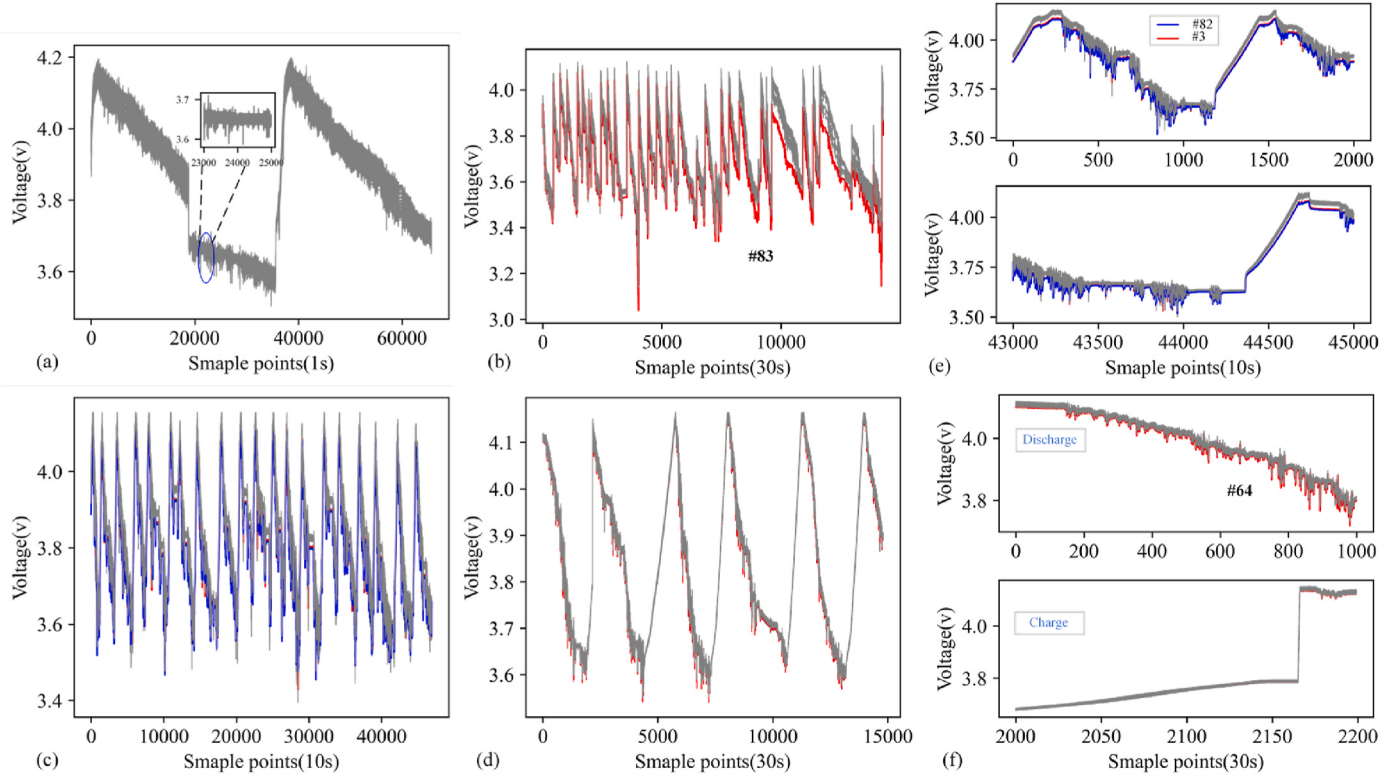


Fig. 5. The voltage diagram of the battery pack. (a) the voltage diagram of Car1; (b) the voltage diagram of Car2; (c) the voltage diagram of Car3; (d) the voltage diagram of Car4; (e) local voltage profile of Car3; (f) local voltage profile of Car4.

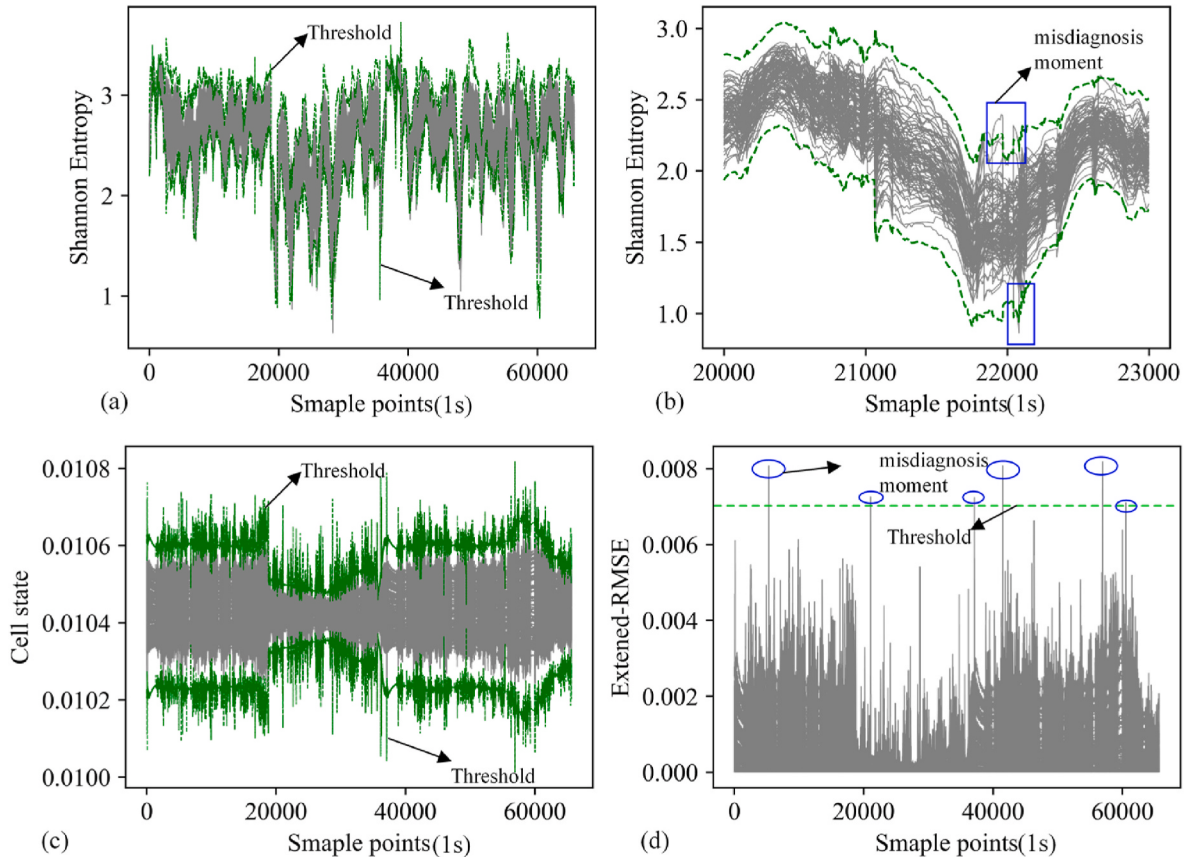


Fig. 6. Fault detection based on three features for Car1. (a) the Shannon entropy of Car1; (b) the partial Shannon entropy diagram of Car1; (c) the Cell state of Car1; (d) the Extended-RMSE of Car1.

cells are lower than the normal voltage. To further analyze the data, samples from the initial moment (0–2000 sampling points) and the end moment (43,000–45,000 sampling points) are carefully examined, as depicted in Fig. 5(e). It is observed that the outliers in the voltage of these two faulty cells do not significantly increase during operation, posing challenges for the fault detection. Fig. 5(d) displays the voltage curve of the battery in Car4, with the red curve representing the voltage curve of battery cell #64. As shown in Fig. 5(f), the malfunction of cell #64 is characterized by capacity degradation and increased internal resistance, which occur throughout both the charging and discharging processes. While no significant voltage anomalies are observed during charging, the voltage remains lower during discharging. This poses a challenge for lithium-ion battery fault diagnosis.

Therefore, all three vehicles examined in this study experienced thermal runaway due to the delayed fault detection for early faults. However, as each vehicle has different triggers for thermal runaway, the

early manifestations of voltage abnormalities also vary accordingly. The voltage deviation of cell #83 in Car2 continues to deepen, while the voltages of cell #3 and cell #82 in Car3 exhibit persistent deviations during charging, but the degrees of deviation do not show significant changes. The voltage of cell #64 in Car4 exhibits a clear pattern of high charging and low discharging, which adds obstacles for fault detection.

In order to validate the necessity of the proposed multi-feature clustering fusion approach in this paper, the information of the battery packs on Car1 and Car2, as mentioned above, is taken as an example to analyze how battery faults can be identified using the three extracted features. After data validation, the Shannon entropy uses a moving window length of $k = 100$, and the Extended RMSE method uses a sliding window length of $N = 10$.

The fault detection results based on three features for Car1 are shown in Fig. 6. Fig. 6(a) illustrates the application of the Shannon entropy method to Car1. The green curves represent the upper and lower limits

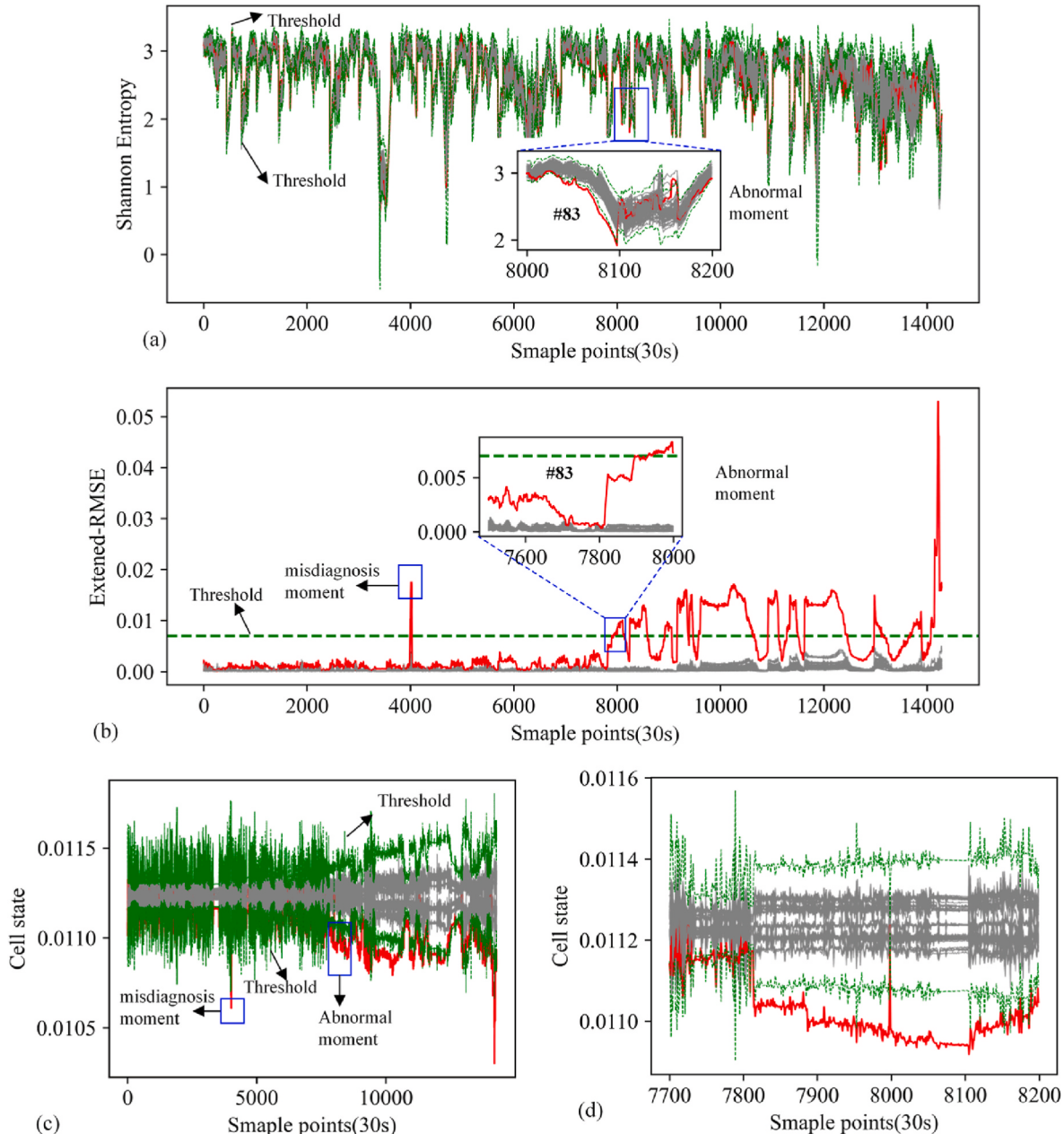


Fig. 7. Fault detection based on three features for Car2. (a) the Shannon entropy of Car2; (b) the Extended RMSE of Car2; (c) the Cell state of Car2; (d) the partial Cell state of Car2.

of the 3σ threshold. Although Car1 is operating normally, applying this method triggers multiple false alarms. For instance, as depicted in Fig. 6(b), false alarms are triggered at 21987th and 22100th sampling moments. These false alarms are attributed to the random voltage perturbations, caused by dynamic operation of vehicles. Fig. 6(c) depicts the results obtained by applying the state SRM method to Car1. The green curves represent the upper and lower limits of the 3σ threshold. No false alarms are detected when utilizing the SRM method for fault detection, indicating its high reliability. Fig. 6(d) displays the application of the Extended RMSE method to Car1. Typically, the Extended RMSE method utilizes the fixed threshold method for fault detection. Taking into account both the accuracy of fault detection and detection time, the fixed threshold of 0.07 is set for this method, but it triggers multiple false alarms.

The fault detection results based on three features for Car2 are shown in Fig. 7. Fig. 7(a) illustrates the application of the Shannon entropy method to Car2. This method shows no significant advantage in fault detection until the 8086th sampling point, which is much longer than the time it takes for the battery voltage to drop significantly. However, this method does not produce any false alarms until the 8086th sampling point. In Fig. 7(b), the results of Car2 applying the Extended RMSE method are shown. The faulty cell is identified at the 7906th sampling point. Based on the earlier description of the battery pack voltage, the significant voltage drop observed in cell #83 at the 4000th sampling point is interpreted as a consequence of deep discharge rather than indicating a fault. Furthermore, the voltage quickly recovered afterwards. Therefore, a misdetection occurs when applying the Extended RMSE method at the 4000th sampling point. Fig. 7(c) illustrates the results obtained by applying the SRM method to Car2. Subsequently, in Fig. 7(d), it is evident that the fault is successfully recognized at the 7822nd sampling point. However, the SRM method also misidentifies the fault at the 4000th sampling point.

In the above results display the fault detection results using the three proposed features individually. The Shannon entropy feature exhibits a sluggish response to fault information, potentially leading to misdetection. On the other hand, the Extended RMSE method demonstrates sensitivity to voltage changes but is prone to a considerable number of misdiagnoses. In contrast, the cell state feature shows sensitivity to specific fault information responses and fewer instances of misdetection. However, it is important to note that for Car2, the fault detection using the SRM method is also delayed. Therefore, individual features often fail to capture sufficient early fault information, leading to delayed detection or frequent misdetection.

3.2. Fault detection based on multi-feature clustering algorithm

In the section 2.3, the DBSCAN algorithm is utilized to conduct cluster analysis on the aforementioned three features in order to identify outliers at each sampling point. And an iterative scoring approach is implemented for each battery cell using a sliding time window. Two parameters of the DBSCAN clustering algorithm, namely Eps and $MinPts$, significantly influence the clustering outcomes. Through extensive data validation, the setting of $Eps = 0.6$ and $MinPts = 3$ is determined, which yields the optimal classification performance. The length of the time window employed for iterative scoring is $L = m$ (the number of individual cells in the battery pack). Adopting such a strategy can mitigate the influence of time window length on the iterative scoring results. Considering both fault detection time and the accuracy of fault detection, for the two-level hierarchical warning, the $threshold_1$ is set to 0.5 and $threshold_2$ is set to 100. These thresholds are determined based on extensive data validation.

3.2.1. Vehicle without fault

The iterative scoring results of each individual cell in Car1 using the proposed method are illustrated in Fig. 8. The green dashed line represents the first-level alarm threshold. Each curve represents the real-time

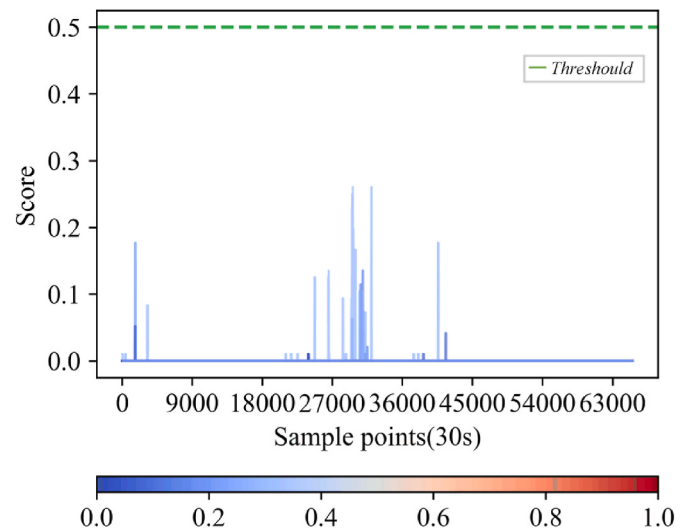


Fig. 8. The score of Car1.

score of each battery cell, transitioning from blue to red indicates a progressively deepening level of fault severity. For Car1, all the cells are represented by a light blue color, indicating that they are fault-free. The analysis of Car1 indicates that, in the absence of faults, the algorithm consistently computes scores for each battery cell well below the pre-defined first-level threshold. This ensures that false alarms are not triggered in the absence of actual faults. This demonstrates that localized sampling errors in voltage measurements have no significant impact on the fault detection results.

3.2.2. Vehicle with early faults

The fault detection results of Car2 using the proposed algorithm are shown in Fig. 9. It can be found that the algorithm successfully identifies the faulty cell #83 at the 349th sampling point. Subsequently, the cumulative sum of cell #83 is tracked. At the 683rd sampling point, it triggers the second-level alarm threshold, confirming cell #83 as the faulty cell. Compared to fault detection based on individual features discussed earlier, the fault detection time is significantly reduced. It is noteworthy that no cases of misdetection are observed throughout the process.

The fault detection results of Car3 using the proposed algorithm is shown in Fig. 10. Fig. 10(a) presents the curve of score values, which fluctuates frequently. Fig. 10(b) and (c) demonstrate that the algorithm successfully identifies faulty cells #3 and #82 at the initial sampling moment. Subsequently, the cumulative sums of the scores for these two cells are tracked, as depicted in Figs. 10(d) and 11(e), which show that cells #3 and #82 trigger the second-level alarm threshold at the 1266th and 1240th sampling points, respectively. The significant fluctuations of the scoring curves for these two faulty cells may be due to the algorithm's reliance on voltage data of individual battery cells. To further enhance the accuracy of fault detection, future research endeavors may consider incorporating additional sensing data, such as battery temperature.

The fault detection results of Car4 using the proposed algorithm is shown in Fig. 11. Fig. 11(a) indicates that the current algorithm successfully identifies the faulty cell #64 at the 467th sampling point. Subsequently, the cumulative sum of the scores for cell #64 is tracked, as shown in Fig. 11(b), determining that at the 6307th sampling point, the second-level alarm is triggered for cell #64, confirming cell #64 as the faulty cell. As the malfunction of Car4's cell #64 is related to capacity degradation and increased internal resistance, significant voltage anomalies do not occur during the charging process. However, during the discharge process, the lower voltage makes the malfunction more pronounced, causing oscillations in the score of cell #64 and leading to a

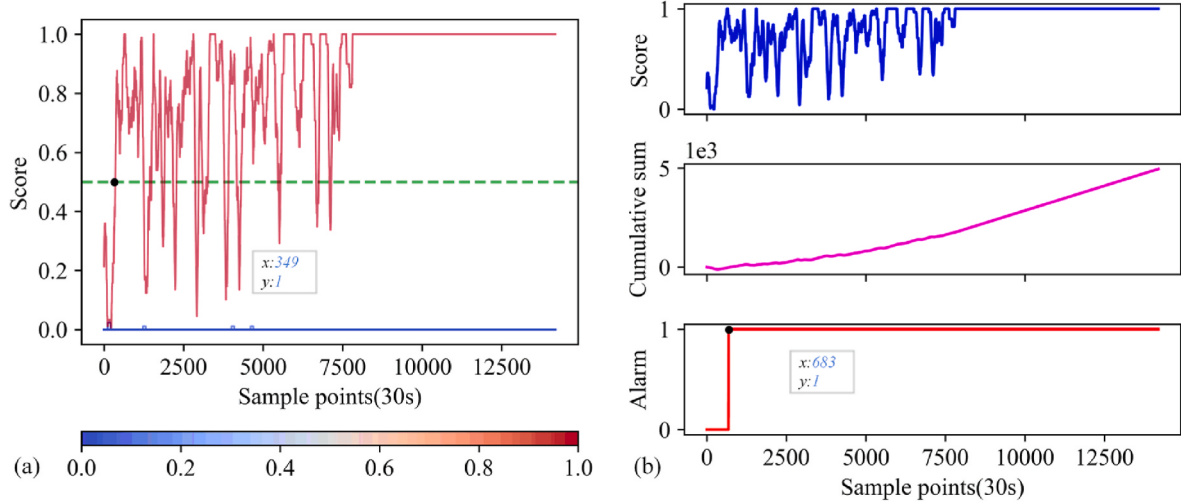


Fig. 9. The results of fault detection for Car2 using the proposed algorithm. (a) the score of Car2; (b) the cumulative sum of cell #83.

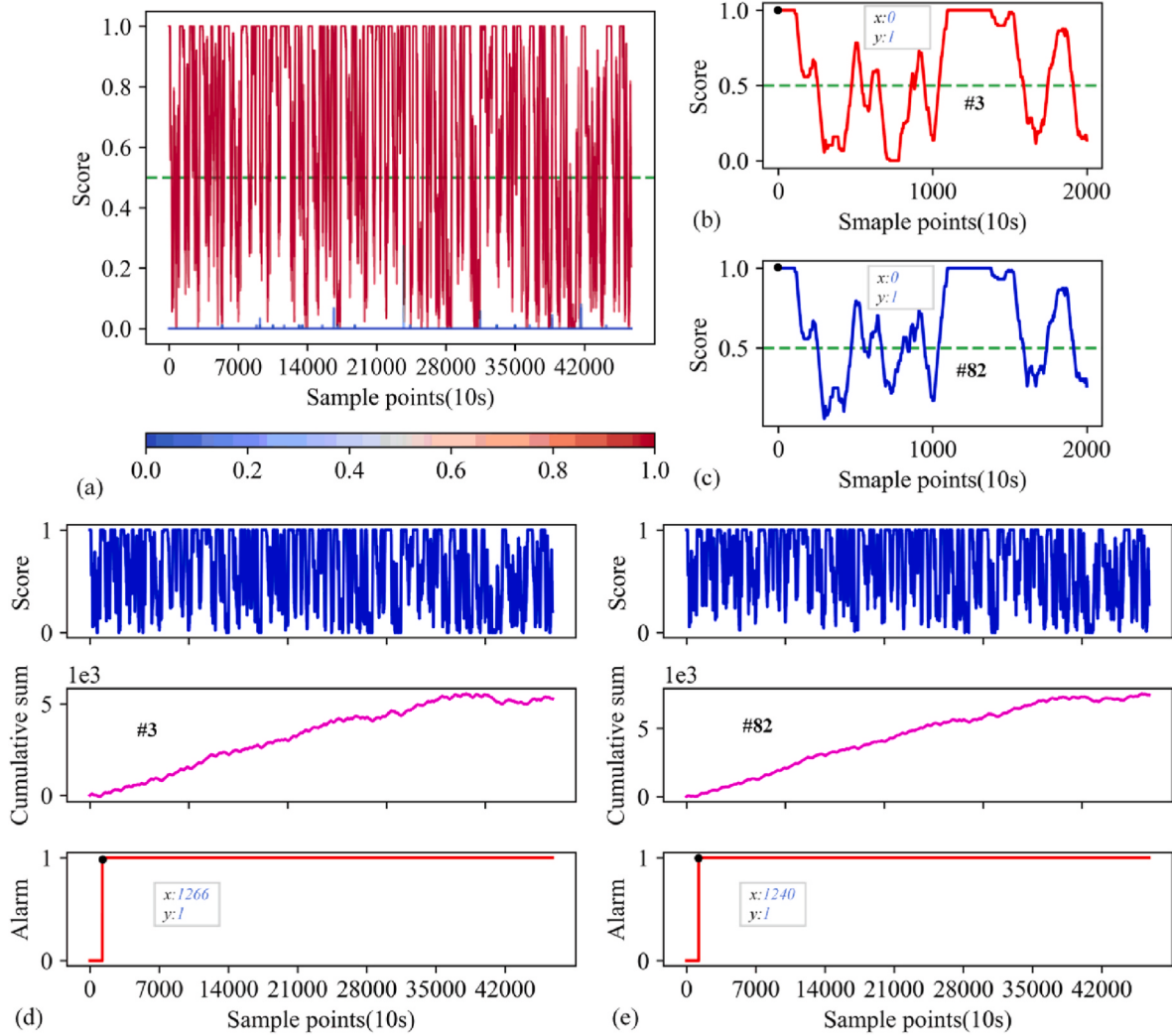


Fig. 10. The results of fault detection for Car3 using the proposed algorithm. (a) the score of Car3; (b) the initial score of cell #3; (c) the initial score of cell #82; (d) the cumulative sum of cell #3; (e) the cumulative sum of cell #82.

delayed determination of fault detection. Nevertheless, there is an improvement in the time taken compared to the BMS alarm time.

As shown in Table 2, it presents a comparative analysis of four fault

detection methods, namely, Shannon entropy, Cell state value, Extended RMSE, and the proposed multi-feature clustering algorithm, and are evaluated across key metrics such as accuracy, false alarm count, and

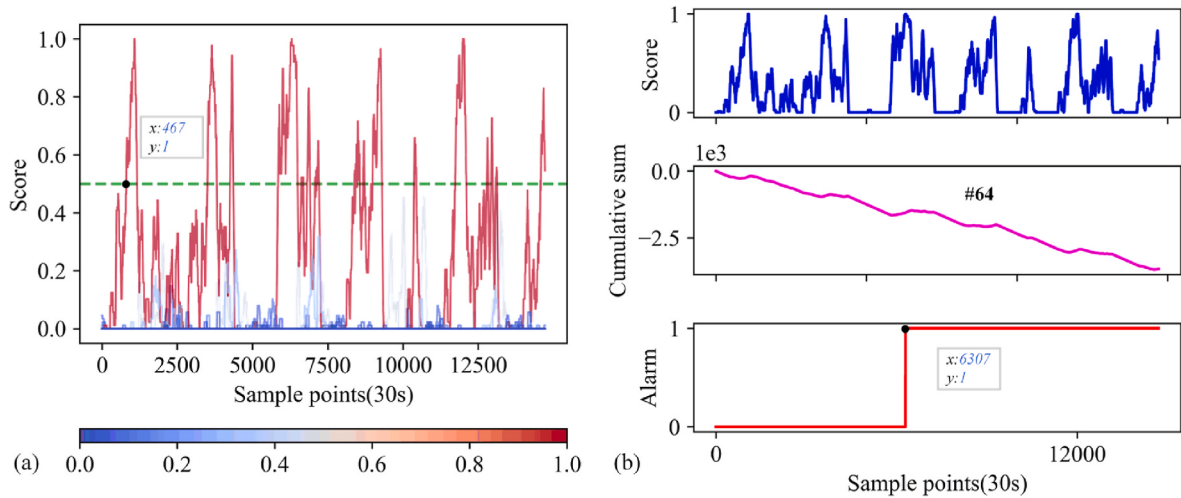


Fig. 11. The results of fault detection for Car4 using the proposed algorithm. (a) the score of Car4; (b) the cumulative sum of cell #64.

Table 2
Comparison between single-feature and multi-feature clustering methods for fault detection.

Method	Accuracy	False Alarm Count	Diagnosis Time (sample points)		
			Car2 (30s)	Car3 (10s)	Car4 (30s)
Shannon entropy	75 %	2567	8086	5156/ 5166	/
Cell state value	75 %	8362	7822	1086/ 1088	/
Extended RMSE	50 %	4055	7906	/	/
Multi-feature Clustering Algorithm	100 %	0	683	1266/ 1240	6307

diagnosis time for different vehicles (Car2, Car3, and Car4). The results indicate that the multi-feature clustering algorithm achieves superior performance with an accuracy of 100%, significantly outperforming the Shannon entropy and Cell state value methods, both of which demonstrate an accuracy of 75%, and the Extended RMSE method, which shows only 50% accuracy. Additionally, the proposed algorithm registers zero false alarms, while the other methods report between 2567 and 8362 false alarms, underscoring its reliability. In terms of diagnosis time, the proposed algorithm detects faults faster than the other methods, with a detection time of 683rd sampling point for Car2's cell #83, 1266th/1240th sampling points for Car3's cell #3 and cell #82, and 6307th sampling point for Car4's cell #64. These results highlight the effectiveness of the proposed algorithm in providing timely and accurate fault detection without producing false alarms and the ability of the algorithm to provide early warnings across vehicles using different sampling frequencies validates its suitability for various sampling rates.

The warning time of the proposed method for different vehicles is shown in Fig. 12. It can be observed that, compared to the alarm time of severe fault identified by the BMS, all three EVs enable early fault warning dozens of days in advance. The variation in alarm times between the BMS and the proposed method stems from several factors: different vehicles exhibit distinct fault types, such as varying self-discharge rates or internal resistance, resulting in diverse early-stage manifestations. Additionally, fault progression varies, with some faults developing rapidly, allowing earlier detection by our algorithm, while others progress more slowly. Finally, the multi-feature clustering algorithm is more sensitive to early fault characteristics, enabling immediate warnings, while traditional BMS triggers alarms only at later stages

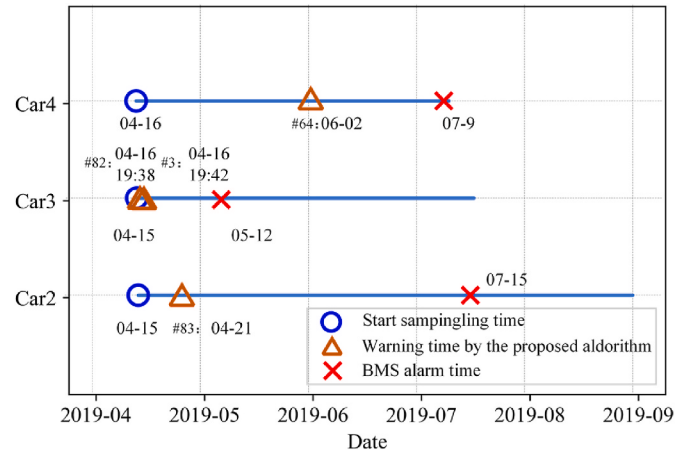


Fig. 12. The comparison results of the warning time.

when anomalies become more pronounced.

The proposed multi-feature clustering fusion algorithm demonstrates its significant practical value for the EV industry. Its unsupervised nature eliminates the need for labeled fault data, making it readily deployable across diverse battery systems. The capability of the algorithm to provide early warnings over ten days in advance of conventional BMS offers manufacturers enough time for preventive maintenance, potentially reducing warranty costs and enhancing vehicle safety. Future applications could extend beyond EVs to stationary energy storage systems and industrial battery arrays. The adaptability of the algorithm to different battery chemistries and configurations, coupled with its real-time monitoring capability, positions it as a promising solution for the BMS. Further research directions could focus on optimizing computational efficiency for large-scale battery pack implementations and incorporating additional sensor modalities to enhance fault discrimination accuracy.

4. Conclusion

With the rapid development of lithium-ion batteries in the field of electrified transportation, the safety issues of batteries are becoming increasingly prominent. Detecting faults early on vehicles can significantly reduce losses. Aiming at this issue, an early fault detection method based on multi-feature clustering fusion for unsupervised scoring and hierarchical warning is proposed in the paper.

Firstly, a feature dataset is proposed to characterize early fault information from various perspectives based on battery cell data. Real-time comprehensive scoring of battery cells is achieved by leveraging clustering algorithms and a sliding window. Subsequently, hierarchical warning for faulty cells is implemented by using the cumulative sum algorithm. Finally, the algorithm's detection and false alarm rates are evaluated using actual failure and normal operation data from the EV's battery packs. High detection rates and low false alarm rates are demonstrated by the algorithm for the four EVs used in this study. Specifically, for the three faulty vehicles, by using each individual feature for fault detection, false alarms or delayed detection are produced. This indicates that relying solely on a certain type of feature for early fault detection of cloud-based data is unreliable. In contrast, utilizing the proposed algorithm for fault detection, faulty cells in the three vehicles can be accurately identified without misdiagnosis, and the time when determining the early battery faults is tens of days ahead of the BMS alarm time. However, this study still has several limitations in various aspects.

- (1) Complexity and Computational Load: The multi-feature clustering and unsupervised scoring process demands considerable computational power, making it well-suited for integration into cloud platforms. However, this may hinder its application in real-time scenarios or systems with limited processing capabilities.
- (2) Limitations in Identifying Fault Types: While the method is effective at detecting anomalies, it has limitations in accurately distinguishing between different types of faults (e.g., internal short circuits, sensor errors, or degradation). The current approach focuses on identifying faulty units but does not provide a clear diagnosis of the underlying cause. Further enhancements would be needed to improve fault type identification.

In the future, our work will focus on introducing multimodal data fusion by integrating data from various sensors, including voltage, current, temperature, and internal pressure, to enhance the accuracy of fault detection, particularly in distinguishing between different fault types.

CRediT authorship contribution statement

Wenhao Nie: Writing – original draft, Visualization, Validation, Software, Methodology, Investigation, Conceptualization. **Zhongwei Deng:** Writing – review & editing, Validation, Supervision, Resources, Methodology, Investigation, Funding acquisition, Conceptualization. **Jinwen Li:** Writing – review & editing, Visualization, Validation, Software, Investigation. **Kai Zhang:** Writing – review & editing, Supervision, Software, Resources, Investigation, Conceptualization. **Jingjing Zhou:** Writing – review & editing, Validation, Supervision, Methodology, Investigation, Conceptualization. **Fei Xiang:** Writing – review & editing, Visualization, Supervision, Resources, Investigation, Conceptualization.

Declaration of competing interest

The authors declare that they have no known competing financial interests or personal relationships that could have appeared to influence the work reported in this paper.

Acknowledgement

This work was supported in part by the National Natural Science Foundation of China (Grant No. 52472401), Sichuan Science and Technology Program (Grant No. 2024NSFSC0938), and China Postdoctoral Science Foundation (Grant No. 2023T160085). The authors gratefully acknowledge the great help of the fund.

Data availability

The authors do not have permission to share data.

References

- [1] Shaffer B, Auffhammer M, Samaras C. Make electric vehicles lighter to maximize climate and safety benefits. *Nature* 2021;598(7880):254–6.
- [2] Dua R, Almutairi S, Bansal P. Emerging energy economics and policy research priorities for enabling the electric vehicle sector. *Energy Rep* 2024;12:1836–47.
- [3] Dua R. Net-zero transport dialogue: emerging developments and the puzzles they present. *Energy for Sustainable Development* 2024;82:101516.
- [4] Martinez N, Terrazas-Santamaria D. Beyond nearshoring: the political economy of Mexico's emerging electric vehicle industry. *Energy Policy* 2024;195:114385.
- [5] Yuan M, Thellufsen JZ, Lund H, Liang YT. The electrification of transportation in energy transition. *Energy* 2021;236:14.
- [6] Jia XY, Zhang CP, Wang LY, Zhang LJ, Zhou XZ. Early diagnosis of accelerated aging for lithium-ion batteries with an integrated framework of aging mechanisms and data-driven methods. *IEEE Transactions on Transportation Electrification* 2022;8(4):4722–42.
- [7] Severson KA, Attia PM, Jin N, Perkins N, Jiang B, Yang Z, et al. Data-driven prediction of battery cycle life before capacity degradation. *Nat Energy* 2019;4(5):383–91.
- [8] Berecibar M, Gudiaga I, Villarreal I, Omar N, Van Mierlo J, Van den Bossche P. Critical review of state of health estimation methods of Li-ion batteries for real applications. *Renew Sustain Energy Rev* 2016;56:572–87.
- [9] Sun P, Bisschop R, Niu H, Huang X. A review of battery fires in electric vehicles. *Fire Technol* 2020;56(4):1361–410.
- [10] Jia X, Zhang C, Wang LY, Zhang L, Zhou X. Early diagnosis of accelerated aging for lithium-ion batteries with an integrated framework of aging mechanisms and data-driven methods. *IEEE Transactions on Transportation Electrification* 2022;8(4):4722–42.
- [11] Hu X, Zhang K, Liu K, Lin X, Dey S, Onori S. Advanced Fault diagnosis for lithium-ion battery systems: a review of fault mechanisms, fault features, and diagnosis procedures. *IEEE Industrial Electronics Magazine* 2020;14(3):65–91.
- [12] Xiong R, Sun W, Yu Q, Sun F. Research progress, challenges and prospects of fault diagnosis on battery system of electric vehicles. *Appl Energy* 2020;279:115855.
- [13] Held M, Brönnimann R. Safe cell, safe battery? Battery fire investigation using FMEA, FTA and practical experiments. *Microelectron Reliab* 2016;64:705–10.
- [14] Zhu X, Wang Z, Wang Y, Wang H, Wang C, Tong L, et al. Overcharge investigation of large format lithium-ion pouch cells with Li(Ni0.6Co0.2Mn0.2)O2 cathode for electric vehicles: thermal runaway features and safety management method. *Energy* 2019;169:868–80.
- [15] Pan F, Ma B, Gao Y, Xu M, Gong D. Parity space approach for Fault diagnosis of lithium-ion battery sensor for electric vehicles. *Automobile Engineering* 2019;41(7):831–8.
- [16] Xiong R, Yu Q, Shen W, Lin C, Sun F. A sensor fault diagnosis method for a lithium-ion battery pack in electric vehicles. *IEEE Trans Power Electron* 2019;34(10):9709–18.
- [17] Ge Y, CZ-q Zheng C. Time-varying parameters estimation and fault diagnosis of li-ion battery using UTSTF. *Journal of ZheJiang University (Engineering Science)* 2018;52(6):1223–30.
- [18] Zhang K, Hu X, Liu Y, Lin X, Liu W. Multi-fault detection and isolation for lithium-ion battery systems. *IEEE Transactions on Power Electronics* 2022;37(1):971–89.
- [19] Xu YM, Ge XH, Shen WX, Yang RX. A soft short-circuit diagnosis method for lithium-ion battery packs in electric vehicles. *IEEE Trans Power Electron* 2022;37(7):8572–81.
- [20] Ng M-F, Zhao J, Yan Q, Conduit GJ, Seh ZW. Predicting the state of charge and health of batteries using data-driven machine learning. *Nat Mach Intell* 2020;2(3):161–70.
- [21] Roman D, Saxena S, Robu V, Pecht M, Flynn D. Machine learning pipeline for battery state-of-health estimation. *Nat Mach Intell* 2021;3(5):447–56.
- [22] Hong J, Wang Z, Liu P. Big-data-based thermal runaway prognosis of battery systems for electric vehicles. *Energies* 2017;10(7):919.
- [23] Wang ZP, Hong JC, Liu P, Zhang L. Voltage fault diagnosis and prognosis of battery systems based on entropy and Z-score for electric vehicles. *Appl Energy* 2017;196:289–302.
- [24] Qiao D, Wang X, Lai X, Zheng Y, Wei X, Dai H. Online quantitative diagnosis of internal short circuit for lithium-ion batteries using incremental capacity method. *Energy* 2022;243:123082.
- [25] Xia B, Shang Y, Nguyen T, Mi C. A correlation based fault detection method for short circuits in battery packs. *J Power Sources* 2017;337:1–10.
- [26] Jiang L, Deng Z, Tang X, Hu L, Lin X, Hu X. Data-driven fault diagnosis and thermal runaway warning for battery packs using real-world vehicle data. *Energy* 2021;234:121266.
- [27] Qiao D, Wei X, Fan W, Jiang B, Lai X, Zheng Y, et al. Toward safe carbon-neutral transportation: battery internal short circuit diagnosis based on cloud data for electric vehicles. *Appl Energy* 2022;317:119168.
- [28] Li D, Deng J, Zhang Z, Wang Z, Zhou L, Liu P. Battery safety risk assessment in real-world electric vehicles based on abnormal internal resistance using proposed robust estimation method and hybrid neural networks. *IEEE Trans Power Electron* 2023;38(6):7661–73.

- [29] Guo W, Yang L, Deng Z, Xiao B, Bian X. Early diagnosis of battery faults through an unsupervised health scoring method for real-world applications. *IEEE Transactions on Transportation Electrification* 2024;10(2):2521–32.
- [30] Li J, Deng Z, Che Y, Xie Y, Hu X, Teodorescu R. Degradation pattern recognition and features extrapolation for battery capacity trajectory prediction. *IEEE Transactions on Transportation Electrification* 2024;10(3):7565–79.
- [31] Sun Z, Liu P, Wang Z. Real-time fault diagnosis method of battery system based on Shannon entropy. *Energy Proc* 2017;105:2354–9.